


Research Article

Structural Changes in the Neonatal Brachial Plexus at Varying Degrees of Stretch

Virginia Orozco¹, Jasmin Jerry¹, Rachel Magee¹, Sriram Balasubramanian¹, Anita Singh^{2*}

Abstract

Neonatal brachial plexus palsy (NBPP) is a common brachial plexus (BP) injury resulting from overstretching of the BP complex during complicated birthing scenarios. Mechanical stretch induced structural changes in nerve tissue include axonal injury, causing cytoskeletal alterations, axonal swelling, and impaired axonal transport and are directly related to dysfunction and degeneration. Limited research exists on the structural changes in the neonatal BP when stretched. This study addresses this gap using a neonatal piglet animal model and investigates the extent of vascular and fiber damage as well as the extent of impaired axoplasmic transport at varying strains in neonatal BP. BP terminal nerves (musculocutaneous, median, ulnar, and radial) were stretched to three strain ranges, namely <10% (mild), 10-20% (moderate), and >20% (severe) strains. All stretched BP terminal nerves had significant changes in their vascular and nerve fiber structure when compared to sham that only underwent surgical procedure. Modified scoring systems for vascular and nerve fiber changes reported vascular and nerve fiber changes to increase with increasing strains. Furthermore, the area of nerve fibers decreased with increasing strain. Axoplasmic transport impairment, measured by beta-amyloid precursor protein (β APP) accumulation at the injury site, also increased with strain. Also, the stretched nerves were significantly differed from sham. This study provides critical insights into strain-induced structural changes in the neonatal BP nerves, highlighting strain dependency in vascular damage, nerve fiber changes, and axoplasmic transport impairments thereby enhancing our understanding of injury severity during NBPP injury.

Keywords: Neonatal brachial plexus; Nerve injury; Strain; Structural changes; Histology; Vascular changes; Nerve fiber changes; Axoplasmic impairment

Abbreviations: NBPP – neonatal brachial plexus palsy; BP – brachial plexus; MSC – musculocutaneous; 3D – three-dimensional; 2D – two-dimensional; H&E – hematoxylin & eosin; NF-IF – neurofilament-immunofluorescence; β APP-IF – beta-amyloid precursor protein-immunofluorescence; PBS – phosphate-buffered saline; OCT – Optimal Cutting Temperature

Introduction

During complicated birthing scenarios, brachial plexus (BP) nerves can be overstretched, resulting in significant injury known as neonatal brachial plexus palsy (NBPP) [1,2]. These BP injuries can present as overstretched (stretched but not ruptured), ruptured (completely broken), avulsed (detached

Affiliation:

¹School of Biomedical Engineering, Science and Health Systems, Drexel University, Philadelphia, Pennsylvania, USA

²Department of Bioengineering, Temple University, Philadelphia, Pennsylvania, USA

*Corresponding Author:

Anita Singh, Department of Bioengineering, Temple University, Philadelphia, Pennsylvania, USA

Citation: Virginia Orozco, Jasmin Jerry, Rachel Magee, Sriram Balasubramanian, Anita Singh. Structural Changes in the Neonatal Brachial Plexus at Varying Degrees of Stretch. *Journal of Orthopedics and Sports Medicine*. 7 (2025): 01-15.

Received: December 19, 2024

Accepted: December 13, 2024

Published: January 09, 2025

from the spinal cord), or combinational injuries [1,3-8]. Despite technological improvements in the field of obstetric care, NBPP continues to significantly impact infants' lives, with a worldwide incidence of 1 to 5 per 1000 live births [1,9-11]. The severity of injury is typically determined after the first three months of birth, where 70-90% of infants with NBPP report spontaneous recovery [1,2,7,12,13], and 30-40% report permanent injury resulting in reduced range of motion with decreased strength, size, and girth of the affected upper extremity [7,8,14]. A recent study reported the incidence of spontaneous recovery of NBPP to be less than previously postulated [15], thereby increasing the need to better understand NBPP injury mechanism and its outcomes.

Axonal injury is a complex pathophysiological process that directly relates to nerve tissue damage and resulting functional impairment. Tensile and shear forces from traumatic mechanisms are the primary cause of axonal injury [16-18]. Axonal injury leads to a variety of structural changes including axonal swelling and cytoskeleton alterations [19]. Several human cadaveric and animal studies have reported mechanical stretch induced structural changes in the nerves, such that varying degrees of stretch lead to varying amounts of nerve tissue damage. Warner et al., 2020 showed that structural damage in adult rat sciatic nerves increased as stretch injury increased [20]. Additional studies have investigated axonal injury induced cytoskeleton alterations and subsequent axonal swelling that directly relates to neuronal dysfunction and degeneration [16-19]. Using the optic nerve from adult guinea pigs, Bain et al., 2000 and 2001 studies reported *in vivo* tissue-level thresholds for axonal injury by comparing the observed structural damage to the estimated tissue strain and displacement, respectively. Singh et al. [27] reported structural changes in adult rat nerve roots at various strains (<10%, 10-20%, and >20%) and strain rates (0.01 mm/sec, 1 mm/sec, and 15 mm/sec). The study used beta-amyloid precursor protein (β APP) and silver impregnation staining techniques to examine the extent of injury as evidence by impaired axoplasmic transport and fiber alignment, respectively, at various strains and strain rates. The silver impregnation technique showed increased spacing and torn or fragmented fibers due to stretch injury at the various strains and strain rates compared to control nerve roots. Furthermore, the rate of occurrence of spacing between fibers and tearing of fibers increased at the higher strain groups. While these studies in adult human tissues and animal models, using various histological techniques, have characterized and quantified the related structural changes at various degrees of stretch, no such studies exist in neonates.

Neonatal nerve injuries can be sustained during traumatic events such as complicated birthing scenarios. Proper diagnosis and treatment of these injuries require a detailed understanding of structural injury mechanisms. This study

aims to address this significant gap by investigating structural changes in the neonatal BP at varying degrees of strain. A neonatal piglet animal model is used to induce varying degrees of stretch to the BP terminal nerves (musculocutaneous, median, ulnar, and radial). Neuroanatomical similarities between piglet and human neonates guide the choice of the animal model used in this study.

Methods

The Drexel University Institutional Animal Care and Use Committee (IACUC) approved all animal procedures. Figure 1 summarizes the presented methodology.

Surgical preparation

Twenty-eight neonatal Yorkshire piglets (3-5 days old) provided the 128 BP nerves (n=32 for each musculocutaneous, median, ulnar, and radial nerve segments) that were used in this *in vivo* study. After a minimum fasting period of 2 hours, piglets were sedated by intramuscular injection of ketamine (20 mg/kg) and xylazine (1.5 mg/kg). Piglets were endotracheally intubated and kept under anesthesia with a mixture of 2.5% isoflurane and a combination of oxygen and nitrous oxide in equal proportions. Intravenous and arterial lines were established in the subcutaneous abdominal vein and femoral artery, respectively. Heart rate, oxygen saturation, core body temperature, and end-tidal carbon dioxide were recorded at 15-minute intervals, and arterial blood gases (pH, pO₂, pCO₂) were collected and evaluated at 30-minute intervals until the end of the experiment.

Surgical procedure

Surgical procedures described previously were used to expose the BP complex bilaterally [21,22]. Briefly, a midline incision was made over the trachea down to the upper third of the sternum with piglets in the spine position and the upper limbs in abduction. Then, the superior and inferior flaps were carefully released, and the BP complex was carefully exposed. The BP was thoroughly examined to identify the bifurcations of the divisions (M shape) and the segments closer to the spine were labeled as root/trunk, and those below the bifurcations were labeled as cord/nerve segments [23]. The four BP terminal nerves (musculocutaneous, median, ulnar, and radial), corresponding to three to four BP nerve root levels, were identified.

In vivo Tensile Biomechanical Testing Device

A custom-built mechanical testing setup previously described by Singh et al. [22,23] was used for *in vivo* stretch of BP nerves. Briefly, the setup included an actuator, a load cell, a custom-made nerve clamp, and a three-dimensional (3D) stereo-camera imaging system. A custom MATLAB (MathWorks, Natick, MA, USA) code controlled the actuator, load cell, and 3D stereo-camera imaging system for synchronous recording.

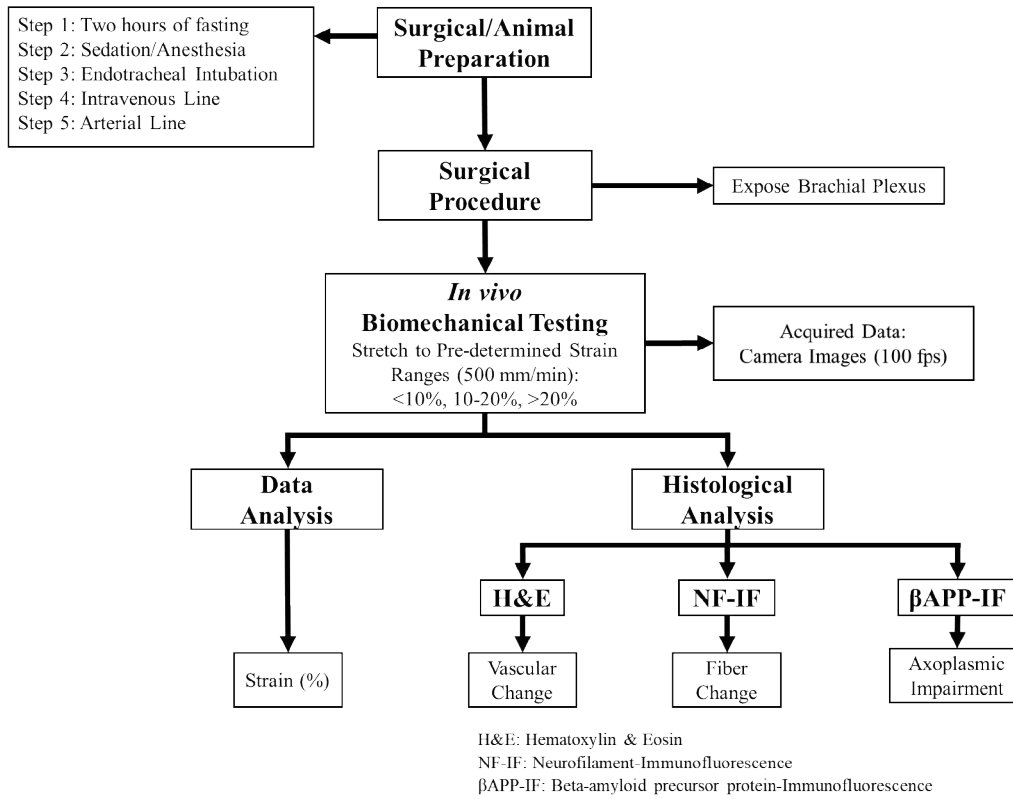


Figure 1: Procedure, data analysis and histological analysis details.

In vivo Tensile Biomechanical Testing

Bilateral *in vivo* tensile biomechanical testing was conducted on each animal. The four BP terminal nerves (musculocutaneous, median, ulnar, and radial) were stretched to three pre-determined strain ranges (<10%, 10-20%, and

>20%) to represent mild, moderate, and severe stretch type, respectively. To achieve pre-determined strain ranges, the initial length of the clamped BP terminal nerve was used to displace the actuator accordingly. Table 1 summarizes testing procedure for each BP terminal nerve stretched to each pre-determined strain range.

Table 1: Table summarizing number of brachial plexus (BP) terminal nerves stretched to three pre-determined strain ranges and corresponding stretch type.

Pre-determined Strain Range	Stretch Type	BP Terminal Nerves			
		Musculocutaneous	Median	Ulnar	Radial
<10%	Mild	8	8	8	8
10-20%	Moderate	8	8	8	8
>20%	Severe	8	8	8	8

The BP terminal nerves were distally cut before stretching and attached to the clamp at the end of the testing setup. Two to four markers were placed along the clamped BP terminal nerve using an ink-based skin marker. The initial length of the clamped BP terminal nerve was measured and used to calculate how much the actuator was displaced to achieve the pre-determined strain ranges. The ZED Mini stereo-imaging camera system was positioned above the clamped BP nerve to capture the displacement of markers during stretch, which were later used to determine 3D tissue strain. The desired

actuator displacement was entered in the custom MATLAB code, and the actuator, load cell, and stereo-imaging camera system were simultaneously activated. The actuator pulled the BP terminal nerve at 500 mm/min until the entered displacement value to achieve the pre-determined strain ranges. The load and displacement data were acquired at 1000 Hz and the camera images were captured at 100 frames per second (FPS). After each test, BP terminal nerves were unclamped and remained attached to their native anatomical site within the body for three hours, except in the high-strain

group, where a complete failure along the length of BP or avulsion occurred. Saline solution was used throughout testing to ensure BP nerves remained hydrated before, during, and after testing.

Strain analysis

As previously described in Orozco et al., 2024, the open-source DLTdv Digitizing Tool [24] was used to track the two-dimensional (2D) displacements of the placed markers of the left and right camera images obtained from the stereo-camera imaging system [25]. The percent strain between each adjacent marker was calculated at each time point until the last frame of the test by dividing the change in length by the initial length and multiplying by 100. The strains between each adjacent marker were averaged to determine the actual strain of the BP terminal nerves stretched to the pre-determined strain ranges.

Tissue preparation

All stretched BP terminal nerves were harvested three hours post-stretch. Four additional animals that only underwent surgical procedures were used to obtain 32 sham BP terminal nerves (eight per each BP terminal nerve: musculocutaneous, median, ulnar, and radial).

The tested (n = 96) and sham (n = 32) BP nerve samples were fixed in 4% paraformaldehyde in phosphate-buffered saline (PBS) for 48 hours. Then, the tissue samples were cryoprotected in 30% sucrose for 48 hours or until the tissue sank to the bottom and embedded longitudinally using the Optimal Cutting Temperature (OCT) compound. 10-µm-thick serial longitudinal sections were processed for hematoxylin & eosin (H&E), neurofilament-immunofluorescence (NF-IF), and beta-amyloid precursor protein-immunofluorescence (βAPP-IF) immunostaining staining using standard protocols [26,27].

Staining

In this study, 384 slides were processed for each staining technique. This included four different BP nerves (musculocutaneous, median, ulnar, and radial), three locations (two peripheries and one center), and three pre-determined strain ranges (<10%, 10-20%, >20%) and sham tissue. Each slide contained 2-4 longitudinal sections. This process was duplicated eight times for each nerve to comprehensively assess 384 slides per staining technique.

Hematoxylin & Eosin (H&E)

Longitudinal sections were stained with standard H&E staining protocol to examine vascular changes of the BP terminal nerves at varying degrees of stretch.

Immunofluorescence Staining

To examine nerve fibers and extent of axoplasmic transport impairment at varying degrees of stretch, longitudinal sections were stained with NF-IF and βAPP-IF, respectively.

Nerve sections were washed twice with deionized water and PBS. The slides were incubated with 10% normal goat serum (Invitrogen, Waltham, MA, USA) to block non-specific binding for 1 hour at room temperature. The sections were then incubated overnight at 4°C in either anti-neurofilament M (1:200, Abcam, Cambridge, UK) antibody, which stains for medium chain proteins, or beta Amyloid Polyclonal (1:100, Invitrogen, Waltham, MA, USA), which stains for beta-amyloid peptides. The sections were then washed three times in PBS and incubated with goat anti-Rabbit IgG, Alexa Flour 488 (Invitrogen, Waltham, MA, USA) for 2 hours at room temperature.

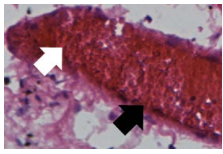
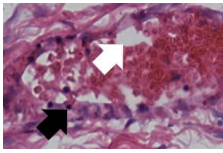
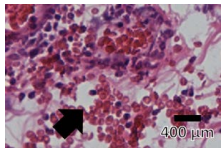
Histological analysis

A blinded observer imaged each longitudinal section along the nerve length from the proximal end to the distal end at 10X magnification using a Leica DMI 4000B microscope (Leica, Wetzlar, Germany). The deidentified image files were saved and used for scoring.

Scoring system for vascular changes

To assess vascular change at varying degrees of stretch, 10X images of H&E-stained slides taken along the nerve length from the proximal to distal end were scored on a scale of 0-2 by an observer blinded to the study design. Table 2 details the modified scoring system used to assess vascular changes. A score of 0 was defined as no to minimal change, where the blood vessel walls remained intact and red blood cells (RBCs) remained compact. A score of 1 was described as moderate change, where the blood vessel wall remained intact, but there was increased spacing between the RBCs. A score of 2 was defined as severe change, where the blood vessel walls ruptured and there were scattered RBCs and/or dispersed RBCs within the tissue.

Table 2: Modified scoring system for vascular changes in the neonatal BP H&E sections.

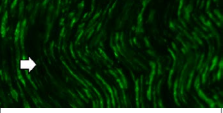
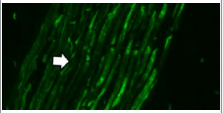
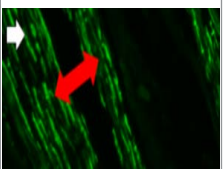
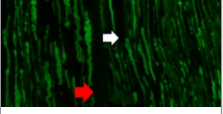
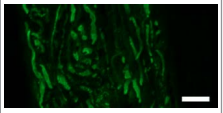
Score Value	Definition	H&E Representative Images	Notations
0	No to minimal change		Intact blood vessel wall (black arrow); compact RBCs (white arrow)
1	Moderate change		Intact blood vessel wall with spacing (black arrow); minimal scattered RBCs (white arrow)
2	Severe change		Broken blood vessel wall with scattered RBCs; dispersed RBCs within tissue (black arrow)

RBCs: Red blood cells. Black scale bar = 400 µm

Scoring system for nerve fiber changes

To assess nerve fiber changes at varying degrees of stretch, 10X images of NF-IF-stained slides taken along the nerve length from the proximal to distal end were scored on a scale of 0-4 by an observer blinded to the study design. Table 3 details the modified scoring system used to evaluate the changes observed in the nerve fibers. A score of 0 was defined as normal where the nerve fibers held their wavy pattern and remained compact. A score of 1 was described as straightening of the nerve fibers where the nerve fibers began to lose their wavy pattern while remaining intact. A score of 2 was defined as increased spacing between the straightened nerve fibers while remaining intact. A score of 3 was defined as fiber fragmentation where the nerve fibers began to break. A score of 4 was defined as complete disruption where the nerve fibers were no longer intact, and the space further increased.

Table 3: Modified scoring system for nerve fiber changes in the neonatal BP NF-IF sections.

Score Value	Definition	NF-IF Representative Images	Notations
0	Normal		The fibers hold their wavy pattern (white arrow) with no increase in space or breakage
1	Straightening of fibers		The uniform wavy pattern begins to straighten (white arrow), while fibers remain intact
2	Increased spacing		The fibers are still intact, with a complete loss of the wavy pattern (white arrow) and an increased amount of spacing (red double arrow)
3	Fiber fragmentation		The fibers begin to fragment (white arrow) while the spacing increases (red arrow)
4	Complete disruption		The fibers are no longer intact with even more space between them

White scale bar = 200 μm

To use the modified scoring system for fiber changes, images were opened in ImageJ (NIH, Bethesda, MD, USA) to add four quadrants. Each quadrant was scored and averaged for an overall score for that image. Figure 2 shows representative 10X NF-IF-stained images of a sham and a stretched sample with four quadrants. In Figure 2A, each quadrant was given a score of 0 for a final average score of 0 for the image of the sham nerve. In Figure 2B, quadrant 1 was scored a 4, quadrants 2 and 3 were scored a 2, and quadrant 4 was scored a 4, for a final average score of 3 for the image of the stretched nerve.

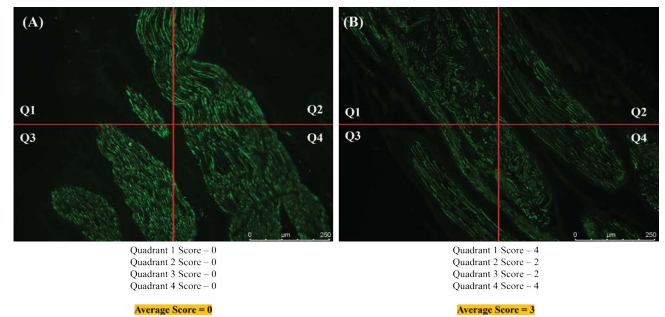


Figure 2: Representative neurofilament-immunofluorescence-stained images of (A) a sham and (B) a stretched brachial plexus terminal nerve. Each image was divided into four quadrants (red lines), scored individually, and averaged for an overall score for that image. The scores for each quadrant and average score (highlighted in yellow) are below each respective image.

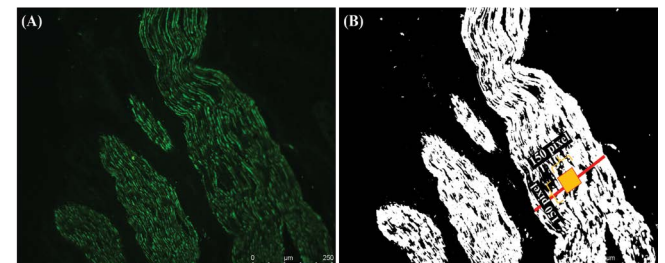


Figure 3: Representative image of a (A) NF-IF image and respective (B) binarized image of the NF-IF image. The widest nerve fascicle was identified, and a 150x150 pixel square box was placed at the center of the widest nerve fascicle. The percent area of the positive NF (white) within the box was measured. NF-IF: Neurofilament-immunofluorescence.

Extent of nerve fiber disruption

The extent of fascicle change was defined as the area of the positive NF staining within the widest nerve fascicle in each 10X image of NF-IF-stained slides taken along the nerve length from the proximal to the distal end. Using ImageJ, a custom macro was created to import the original image (Figure 3A), binarize the imported image (Figure 3B), and set a universal threshold. The widest fascicle was identified by measuring the diameters of each visible fascicle within each

image. A 150x150 pixel square box was placed at the center of the widest nerve fascicle. The percent area of the positive NF within the 150 ×150 pixel box was measured.

Extent of axoplasmic transport impairment

The extent of axoplasmic transport impairment was defined as the positive βAPP accumulation within each 10X image of βAPP-IF-stained slides taken along the nerve length from the proximal to the distal end. Using ImageJ, a custom macro was created to import the original image (Figure 4A), binarize imported image (Figure 4B), and set a universal threshold. A 150x150 pixel square box was placed in the region with the most positive βAPP, if any, that was green in the original image and now white in the binarized image (Figure 4B). The percent area of the positive βAPP within the 150x150 pixel square box was measured.

Statistical analysis

SPSS software version 29 (IBM, Armonk, NY, USA) was used to perform statistical analysis. The structural changes observed by vascular score, nerve fiber score, percent nerve fiber area, and percent βAPP accumulation are reported as mean ± standard deviation (mean ± SD). A Shapiro-Wilk test for normality was performed and determined that vascular score, nerve fiber score, percent nerve fiber area, and percent βAPP accumulation did not follow a normal distribution. A non-parametric Kruskal-Wallis test followed by a

Bonferroni post-hoc test was performed to assess how the two independent factors influenced the structural changes: location (two peripheries and one center) and strain ranges (<10%, 10-20%, and >20%). The significance level was set at $p < 0.05$.

Results

A total of 96 BP terminal nerves, 24 per each BP terminal nerve (musculocutaneous, median, ulnar, and radial) and 8 per strain ranges (<10%, 10-20%, and >20%) and additional 8 shams per BP terminal nerve. The sham samples only underwent surgical procedures with no biomechanical testing. The stretched BP terminal nerves were grouped based on their actual measured strain from the pre-determined strain tests and grouped in the strain ranges and corresponding stretch types. Table 4 details the total number of BP terminal nerves within each strain range and their average measured strains (shown in mean ± standard deviation).

Histological findings

The 96 tested BP terminal nerves plus the 32 shams samples (8 per BP terminal nerve) were processed for qualitative and semi-quantitative histological assessment. Three longitudinal slides, two from the periphery and one from the center with 2-4 longitudinal sections for each BP terminal nerve at each strain group plus sham were stained with H&E, NF-IF, and βAPP-IF to assess vascular change,

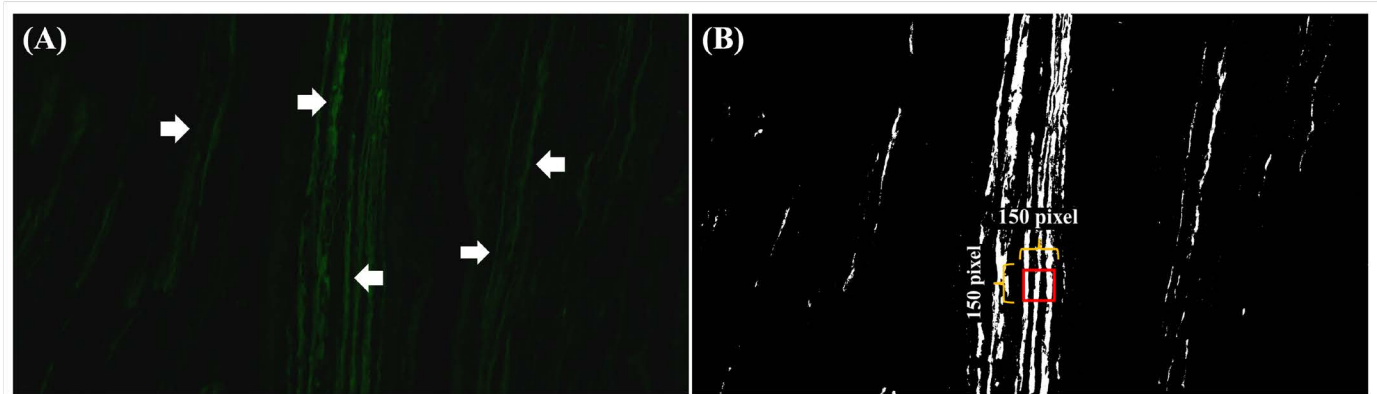


Figure 4: Representative image of a (A) βAPP-IF image and respective (B) binarized image of the βAPP-IF image. A 150×150 pixel square box was placed in the region with the most positive βAPP, if any. The percent area of the positive βAPP within 150×150 pixel square box was measured. βAPP-IF: Beta-amyloid precursor protein-immunofluorescence.

Table 4: Summary table shows the total number of tested brachial plexus terminal nerves per strain range, stretch type, and average measured strains.

Brachial Plexus Terminal Nerves					
Strain Ranges	Stretch Type	Musculocutaneous	Median	Ulnar	Radial
<10%	Mild	4.8±2.5% (n = 8)	6.1±2.4% (n = 8)	5.1±2.0% (n = 8)	3.9±1.8% (n = 8)
10-20%	Moderate	12.5±2.2% (n = 8)	14.9±3.0% (n = 8)	13.3±3.0% (n = 8)	11.6±1.5% (n = 8)
>20%	Severe	27.1±5.4% (n = 8)	45.8±38.8% (n = 8)	32.3±10.5% (n = 8)	51.1±14.8% (n = 8)

Values are reported as mean ± standard deviation.

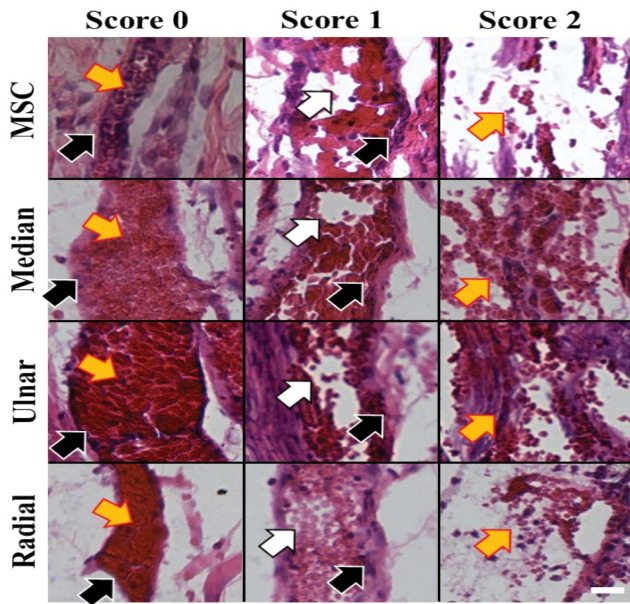


Figure 5: Representative hematoxylin & eosin images of observed vascular changes scored on a scale of 0-2 for each brachial plexus terminal nerve. Black arrow with white outline shows intact blood vessel walls and yellow arrow with red outline shows compact red blood cells together defining a score of 0. Black arrow with white outline shows intact blood vessel walls and white arrow with black outline shows increased spacing between red blood cells, indicating a score of 1. A yellow arrow with red outline shows a broken blood vessel wall with scattered red blood cells representing a score of 2. MSC: Musculocutaneous. White scale bar = 400 μ m.

nerve fiber change and extent of fiber disruption, and extent of axoplasmic transport impairment, respectively.

Increasing stretch increased the observed vascular changes

H&E-stained slides were examined for any vascular change as defined by the modified scoring system described in Table 2. The modified scoring system showed that as stretch increased, the observed vascular changes increased for each BP terminal nerve (musculocutaneous, median, ulnar, and radial). Figure 5 shows representative images of the observed vascular changes scored 0-2 for each BP terminal nerve.

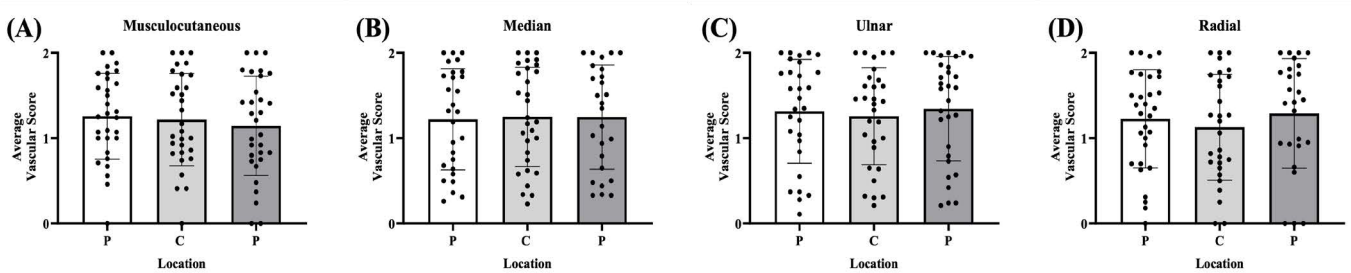


Figure 6: Bar graphs of mean \pm standard deviation of average vascular score at the two peripheries (P) and one center (C) of (A) musculocutaneous, (B) median, (C) ulnar, and (D) radial brachial plexus terminal nerves. Solid black circles represent each data point for that location. Error bars represent plus and minus standard deviation.

Vascular changes with respect to location

For each BP terminal nerve, two slides from the peripheries (P) and one from the center (C) were examined from the shams and stretch groups mild, moderate, and severe that correspond to the strain ranges <10%, 10-20%, and >20%, respectively. No significant differences in vascular changes were found between the two periphery sections and the one center section of the musculocutaneous ($p = 0.75$, Figure 6A), median ($p = 0.97$, Figure 6B), ulnar ($p = 0.51$, Figure 6C), and radial ($p = 0.43$, Figure 6D) BP terminal nerves stretched at various strains.

Vascular changes with respect to strain range

The observed vascular change increased with increasing strain in all BP terminal nerves (musculocutaneous, median, ulnar, and radial). In the musculocutaneous (Figure 7A), median (Figure 7B), ulnar (Figure 7C), and radial (Figure 7D) BP terminal nerves, the sham was significantly different from the three stretch groups. It was also found that in the musculocutaneous (Figure 7A) and radial (Figure 7D) BP terminal nerves the severe stretch group was significantly greater than the mild and moderate stretch groups. In the median (Figure 7B) and ulnar (Figure 7C) BP terminal nerves the severe stretch group is only significantly greater than the mild stretch group. In the median (Figure 7B) BP terminal nerve the moderate stretch group was significantly greater than the mild stretch group.

Increasing stretch increased the observed nerve fiber changes

NF-IF-stained slides were examined for nerve fiber changes as defined by the modified scoring system described in Table 3. The modified scoring system showed that nerve fiber changes increased with increasing strain for each BP terminal nerve (musculocutaneous, median, ulnar, and radial). Figure 8 shows representative images of nerve fiber changes scored on a scale of 0-4 for each BP terminal nerve.

Nerve fiber changes with respect to location

For each BP terminal nerve, two slides from the peripheries (P) and one from the center (C) were examined from the

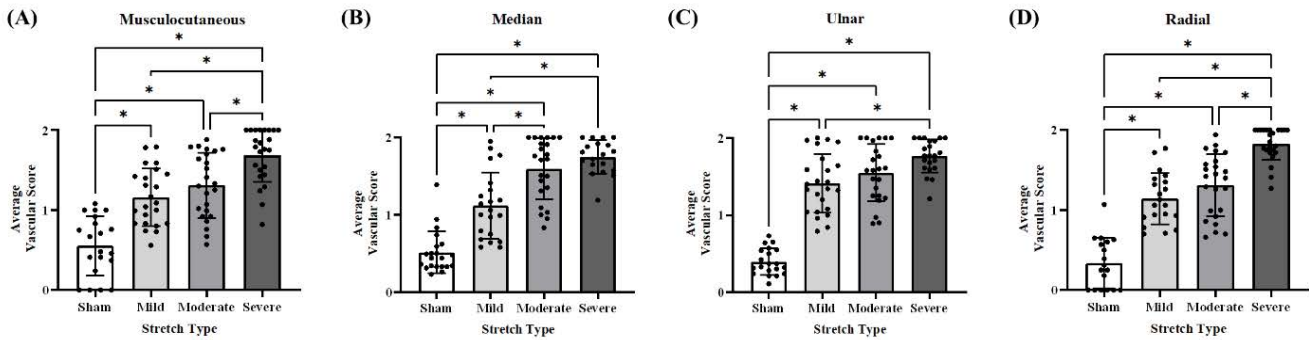


Figure 7: Bar graphs of mean \pm standard deviation of average vascular score of (A) musculocutaneous, (B) median, (C) ulnar, and (D) radial brachial plexus terminal nerves stretched to <10%, 10-20%, and >20% strain ranges to represent mild, moderate, and severe stretch types, respectively, plus sham samples. Error bars represent plus and minus standard deviation. Solid black circles represent each data point. *: $p < 0.05$.

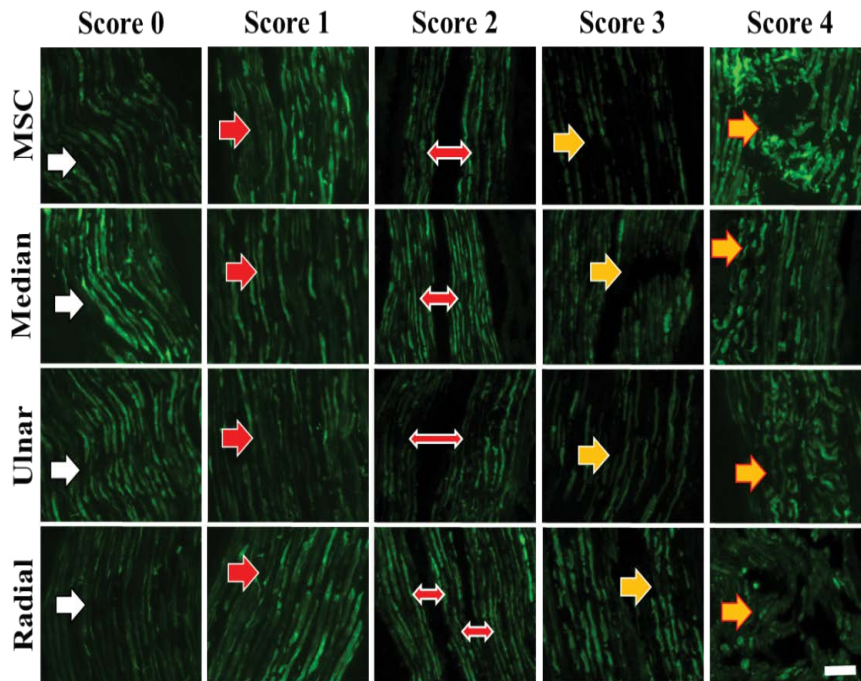


Figure 8: Representative neurofilament-immunofluorescence images showing observed nerve fiber changes scored on a scale of 0-4 for each brachial plexus terminal nerve. White arrow shows wavy pattern representative of score 0. A red arrow with a white outline show straightening of fibers indicating a score of 1. Double red arrow with white outline shows increasing spacing between fibers defining a score of 2. Yellow arrow with white outline shows fiber fragmentation representing a score of 3. Yellow arrow with red outline shows complete disruption defining a score of 4. MSC: Musculocutaneous. White scale bar = 200 μ m.

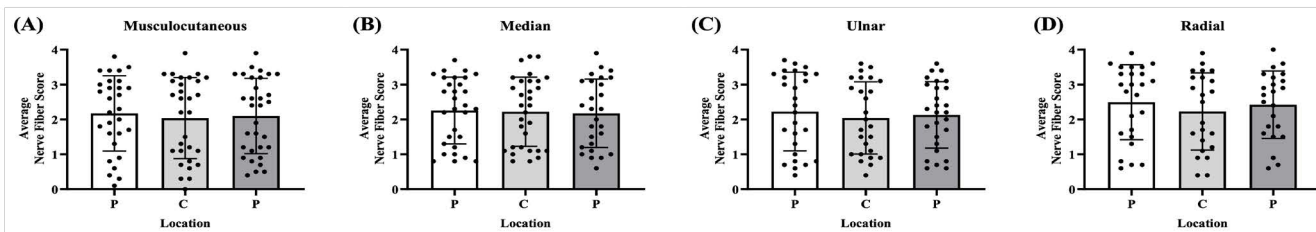


Figure 9: 1 Bar graph of mean \pm standard deviation of average nerve fiber score at the two peripheries (P) and one center (C) of (A) musculocutaneous, (B) median, (C) ulnar, and (D) radial BP terminal nerves. Solid black circles represent each data point for that location. Error bars represent plus and minus standard deviation.

shams and stretch groups mild, moderate, and severe that correspond to the strain ranges <10%, 10-20%, and >20%, respectively. No significant differences in the average nerve fiber score were found between the two periphery sections and one center section of the musculocutaneous ($p = 0.30$, Figure 9A), median ($p = 0.90$, Figure 9B), ulnar ($p = 0.10$, Figure 9C), and radial ($p = 0.32$, Figure 9D) BP terminal nerves at the varying degrees of stretch.

Nerve fiber changes with respect to strain range

The average nerve fiber score significantly differed between the sham and stretch groups for each BP terminal nerve (musculocutaneous, median, ulnar, and radial). In the musculocutaneous (Figure 10A), median (Figure 10B), ulnar

(Figure 10C), and radial (Figure 10D) BP terminal nerves, the sham was significantly different from the three stretch groups. For all the BP terminal nerves, it was found that the average nerve fiber score in the moderate stretch group was significantly greater than the mild (Figure 10A-D) stretch group and the average nerve fiber score in the severe stretch was significantly greater than the mild (Figure 10A-D) and moderate (Figure 10A-D) stretch groups.

Percent nerve fiber area decreased with increasing stretch

NF-IF-stained slides were examined for extent of fascial damage by measuring the percent of nerve fiber area within the widest fascicle. As stretch increased, the percent of

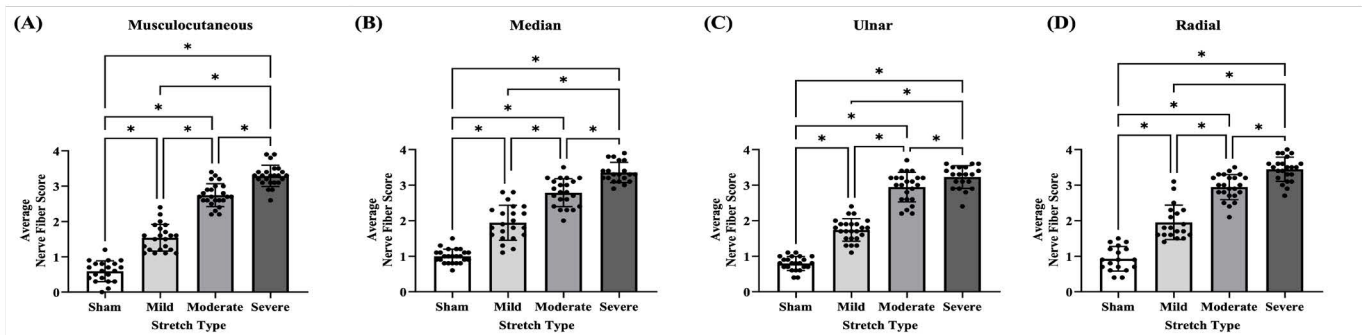


Figure 10: Bar graphs of mean \pm standard deviation of average nerve fiber score of (A) musculocutaneous, (B) median, (C) ulnar, and (D) radial brachial plexus terminal nerves stretched to <10%, 10-20%, and >20% strain ranges to represent mild, moderate, and severe stretch types, respectively, plus sham samples. Error bars represent plus and minus standard deviation. Solid black circles represent each data point. *: $p < 0.05$.

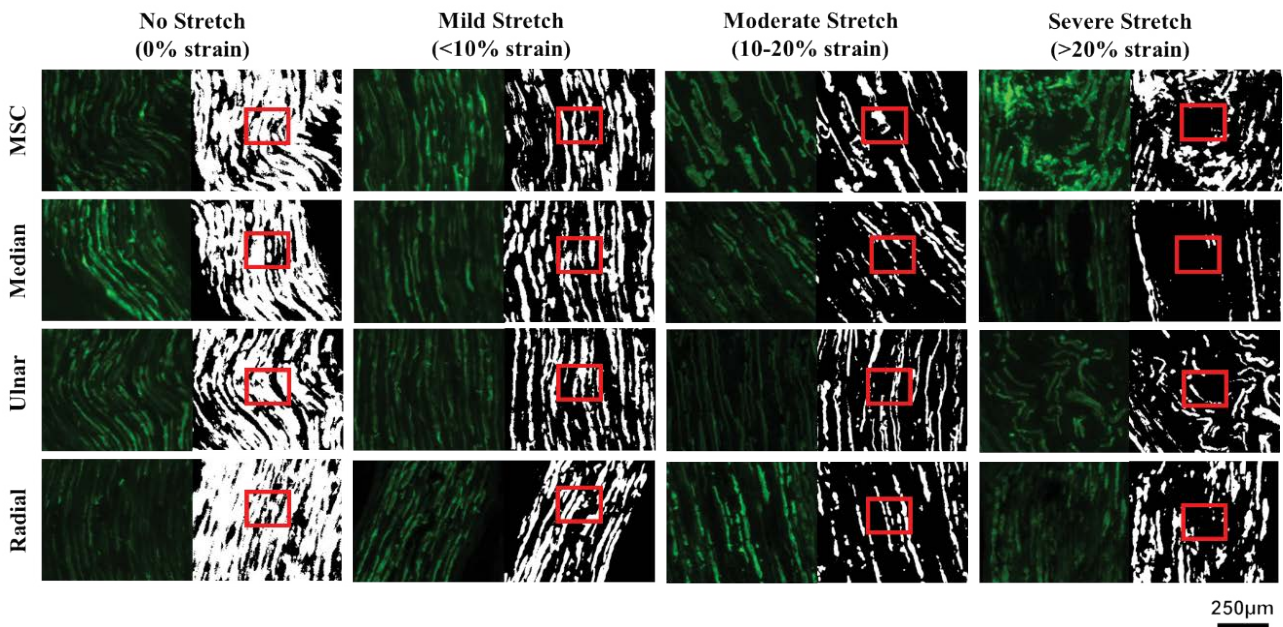


Figure 11: Representative neurofilament-immunofluorescence images (left) and respective binary image (right) of brachial plexus levels (musculocutaneous, median, ulnar, and radial) at various degrees of strains (0%, <10%, 10-20%, and >20%) to represent no, mild, moderate, and severe stretch, respectively. The red box represents a region of interest where nerve fiber area was measured to evaluate extent of fascicle changes at various degrees of stretch. MSC: musculocutaneous. Black scale bar = 250 μ m.

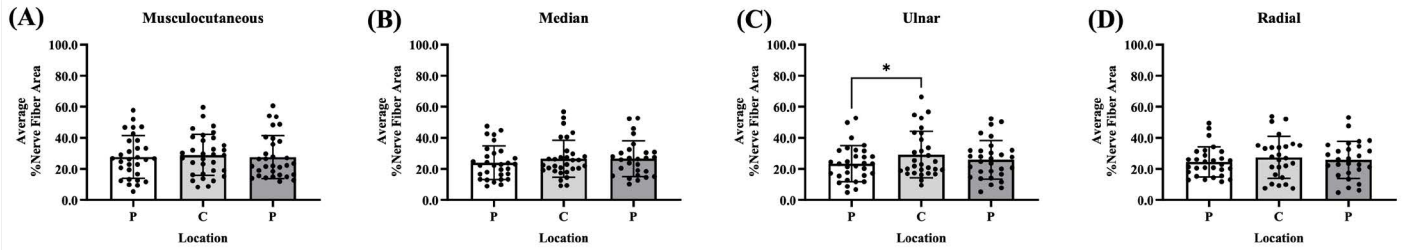


Figure 12: Bar graphs of mean \pm standard deviation of average percent nerve fiber area at two peripheries (P) and one center (C) of (A) musculocutaneous, (B) median, (C) ulnar, and (D) radial BP terminal nerves. Solid black circles represent each data point for that location. Error bars represent plus and minus standard deviation. *: $p < 0.05$.

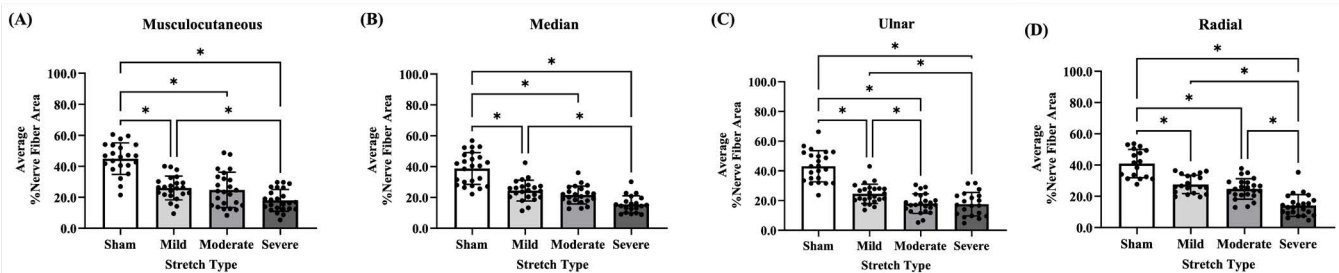


Figure 13: Bar graph of mean \pm standard deviation of average percent nerve fiber area of (A) musculocutaneous, (B) median, (C) ulnar, and (D) radial brachial plexus terminal nerves stretched to $<10\%$, $10-20\%$, and $>20\%$ strain ranges to represent mild, moderate, and severe stretch types, respectively, plus sham samples. Error bars represent plus and minus standard deviation. Solid black circles represent each data point. *: $p < 0.05$.

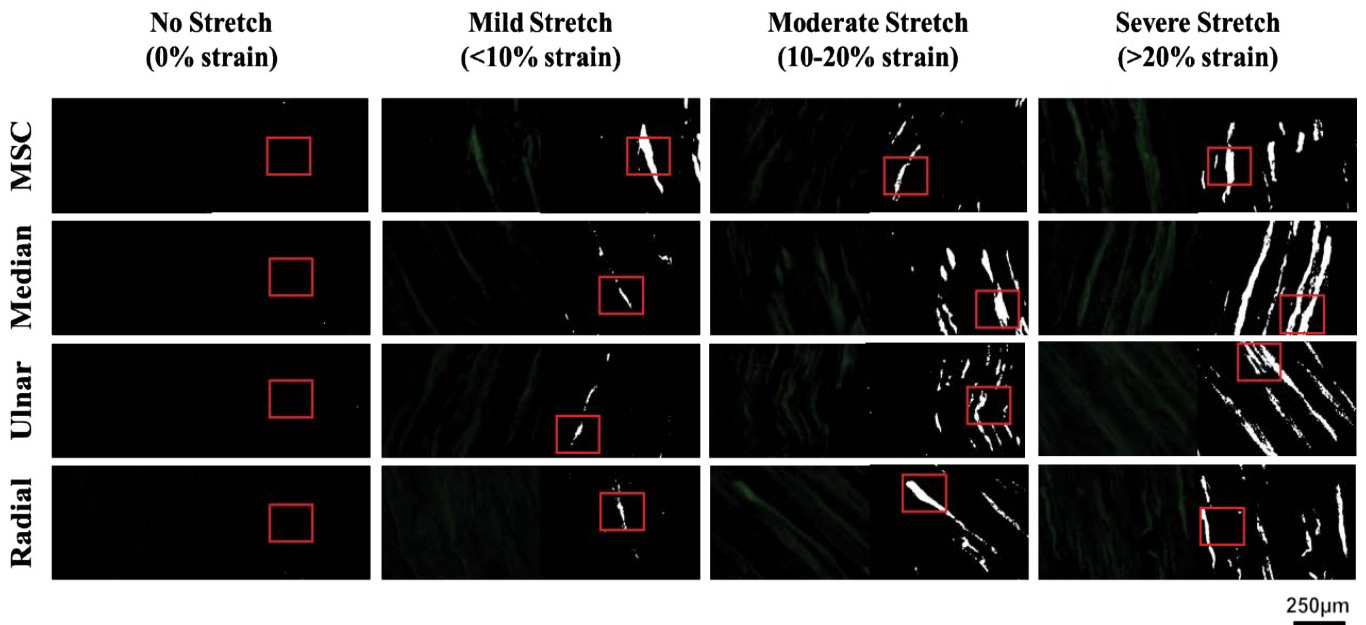


Figure 14: Representative beta-amyloid precursor protein-immunofluorescence (left) images and respective binary images (right) of brachial plexus levels (musculocutaneous, median, ulnar, and radial) at various degrees of strains (0% , $<10\%$, $10-20\%$, and $>20\%$) to represent no, mild, moderate, and severe stretch, respectively. The red box on binarized image represents a region of interest where the amount of beta-amyloid precursor protein was measured to examine extent of axoplasmic transport impairment at various degrees of stretch. MSC: musculocutaneous. Black scale bar = $250 \mu\text{m}$.

nerve fiber area within the widest fascicle decreased for each BP terminal nerve (musculocutaneous, median, ulnar, and radial). Figure 11 shows representative images of NF-IF stained slides with their respective binarized image for each BP terminal nerve (musculocutaneous, median, ulnar, and radial) at the various strain ranges (<10%, 10-20%, and >20%) to represent mild, moderate, and severe stretch, respectively, plus sham (no stretch).

Extent of Fascicle Changes with respect to Location

For each BP terminal nerve, two slides from the peripheries (P) and one from the center (C) were examined from the shams and stretch groups mild, moderate, and severe that correspond to the strain ranges <10%, 10-20%, and >20%, respectively. No significant differences in the average nerve fiber score were found between the two periphery sections and one center section of the musculocutaneous (p = 0.30, Figure 12A), median (p = 0.90, Figure 12B), and radial (p = 0.32, Figure 12D) BP terminal nerves. Significant differences between one periphery and the center were found in the ulnar BP terminal nerve (p < 0.05, Figure 12C).

Extent of fascicle changes with respect to strain range

The average percent nerve fiber area significantly differed with respect to strain for each BP terminal nerve. In the musculocutaneous (Figure 13A), median (Figure 13B), ulnar (Figure 13C), and radial (Figure 13D) BP terminal nerves, the sham significantly differed from the three stretch groups. In the musculocutaneous (Figure 13A) and median (Figure 13B) BP terminal nerves the severe stretch group was significantly less than the mild stretch group. In the ulnar (Figure 13C) and radial (Figure 13D) the mild stretch group was significantly greater than the moderate and severe stretch groups.

βAPP accumulation increased with increasing stretch

βAPP-stained slides were used to examine the extent of axoplasmic transport impairment by measuring the amount

of positive βAPP. It was found that the amount of positive βAPP increased as the strain increased. Figure 14 shows representative images of βAPP-IF stained slides with their respective binarized image for each BP terminal nerve (musculocutaneous, median, ulnar, and radial) at various strain ranges (<10%, 10-20%, and >20%).

βAPP accumulation with respect to location

For each BP terminal nerve, two slides from the peripheries (P) and one from the center (C) were examined from the shams and stretch groups mild, moderate, and severe that correspond to the strain ranges <10%, 10-20%, and >20%, respectively. No significant differences in βAPP accumulation were found between the two periphery sections and one center section of the musculocutaneous (p = 0.16, Figure 15A), median (p = 0.83, Figure 15B), ulnar (p = 0.84, Figure 15C), and radial (p = 0.63, Figure 15D) BP terminal nerves at the varying degrees of stretch type.

βAPP accumulation with respect to strain range

βAPP accumulation was significantly different between sham and stretch groups for each BP terminal nerve. In musculocutaneous (Figure 16A) and median (Figure 16B) BP terminal nerves, sham significantly differed from the three stretch groups. In the ulnar (Figure 16C) and radial (Figure 16D) BP terminal nerves, sham significantly differed from only moderate and severe stretch groups. The average percent of positive βAPP was significantly less in the mild stretch group compared to the severe stretch groups in the musculocutaneous (Figure 16A), ulnar (Figure 16C), and radial (Figure 16D). In the median BP terminal nerve, there were no significant differences between the three stretch groups (Figure 16B). In the ulnar BP terminal nerve, the average percent of positive βAPP was significantly less in the mild stretch group compared to the moderate stretch group (Figure 16C). The average percent of positive βAPP was significantly less in the moderate stretch group compared to the severe stretch group in the radial BP terminal nerve (Figure 16D).

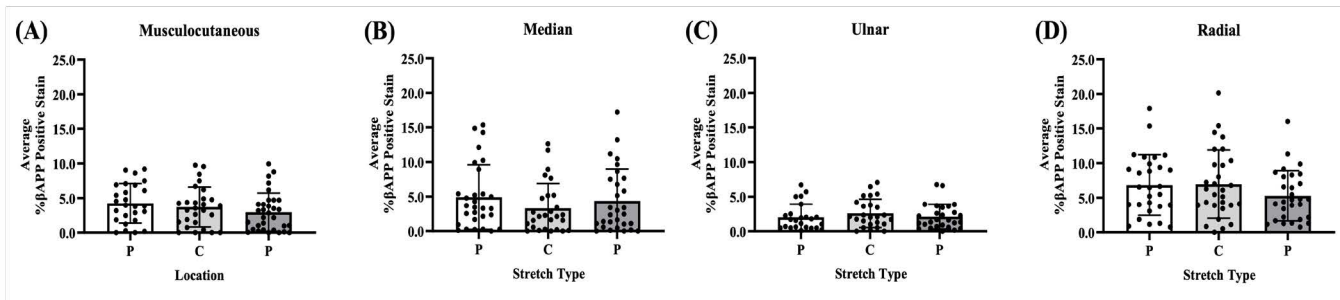


Figure 15: Bar graphs of mean ± standard deviation of average beta-amyloid precursor protein accumulation at two peripheries (P) and one center (C) of (A) musculocutaneous, (B) median, (C) ulnar, and (D) radial brachial plexus terminal nerves. Solid black circles represent each data point for that location. Error bars represent plus and minus standard deviation.

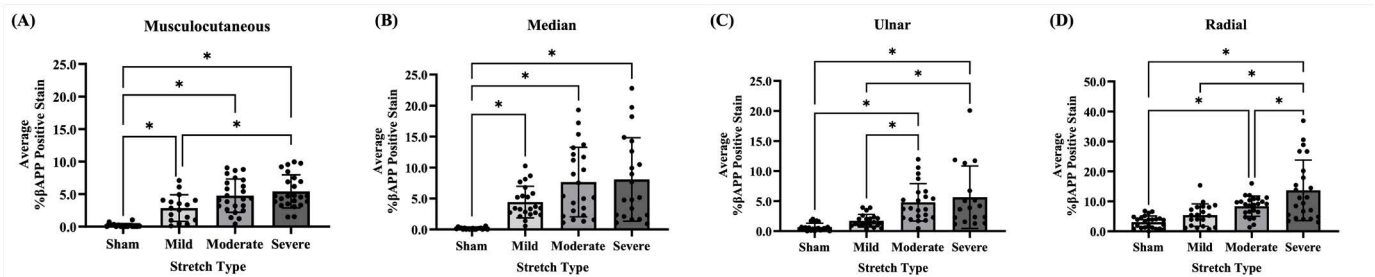


Figure 16: Bar graph of mean ± standard deviation of average percent of positive beta-amyloid precursor protein of (A) musculocutaneous, (B) median, (C) ulnar, and (D) radial brachial plexus terminal nerves stretched to <10%, 10-20%, and >20% strain ranges to represent mild, moderate, and severe stretch types, respectively, plus sham samples. Error bars represent plus and minus standard deviation. Solid black circles represent each data point. *: $p < 0.05$.

Discussion

This study is the first to characterize the related structural changes of the neonatal BP when subjected to varying degrees of stretch in a clinically relevant neonatal piglet animal model. Currently there is limited available morphological data characterizing the BP let alone the neonate BP due to stretching. It is known that strain is the primary factor of axonal injury in peripheral nerves [16-18]. Using data and methodology of the available studies as a foundation, this study examined vascular changes, nerve fiber changes and extent of fascial change, and extent of axoplasmic impairment in neonatal BP nerve tissue at various strains using H&E, NF-IF, and β APP-IF histological techniques, respectively [26,27].

The peripheral nerve vasculature helps regulate the microenvironment by supplying oxygen, nutrients, and waste removal to ensure proper function and health of the peripheral nerves [28-32]. Therefore, understanding how the vasculature of peripheral nerves changes with respect to various degrees of strains can provide insight into the functional health of peripheral nerves. In this current study, using a modified scoring system, it was found that as strains increased the vascular change increased. The results showed that sham samples also observed minimal vascular change, which can be attributed to damage during handling the tissue during the surgical procedure. Despite this, the sham samples were significantly different from the stretched samples. Furthermore, for the four tested BP terminal nerves (musculocutaneous, median, ulnar, and radial), it was found that the <10% strain group (mild stretch type) was different from the other strain groups (10-20% and >20%). Significant difference in even the <10% group when compared to sham implies that vascular change in neonatal BP tissue can occur at strains lower than 10%. Jo et al., 2000 reported vascular changes, specifically congestions of epineural vessels and inflammation, were first observed histologically at 24% strain although blood flow reduction was observed at 8% strain [33]. Compared to the current study, Jo et al. [33] reported higher strain of observing vascular changes using histological

techniques can be attributed to the type of nerve used (sciatic nerve) and the type of animal model (adult rat animal model).

Neurofilaments (NFs) are a structural component of the neuron's cytoskeleton. NFs are a dominant intermediate filament of the axons that primarily provide structural support [16,34]. These filaments not only provide structural support, but support axonal and dendritic growth and are involved in the axoplasmic transport [16,35]. Therefore, any change to the integrity of nerve fascicles from stretching can lead to nerve fiber disruption, ultimately affecting the neuron structural integrity. In the current study, a modified scoring system was implemented to score NF-IF-stained slides of the BP terminal nerves (musculocutaneous, median, ulnar, and radial) at various degrees of stretch. It was found that compared to the sham samples, which only underwent the surgical procedure, the stretched samples were significantly different for each BP terminal nerve. Additionally, it was found that as stretching increased, the nerve fiber changes increased. Singh et al. [26,27] found that as stretch increased the occurrence of nerve fiber damage in adult rat nerve roots increased. Although a direct comparison cannot be made between the two studies and the current study, all three studies conclude that as stretch increased the degree of structural changes to nerve fibers increased. Warner et al. [20] examined the rapid-stretch injury response of adult rat sciatic nerves and found that as stretch increased the nerves began to lose their wavy, compact pattern and more occurrences of micro-ruptures were observed. Mahan et al. [36] also found that as stretch increased nerve fiber damage increased in adult rat sciatic nerves. They further found that at mild stretches that corresponded to strains <15% axons remained intact with signs of loss of nerve fiber undulation (wavy pattern). In the current study, loss of the undulation pattern in neonatal BP terminal nerves was first observed at strains <10%. The difference can be attributed to the animal model used (adult small animal model vs neonatal large animal model), testing methodology, and histological assessment.

The extent of fascicle change was examined by measuring the percent area of a region of interest (ROI) at the widest

nerve fascicle. It was found that as stretch increased, the percent area of nerve fibers within the ROI decreased. Because nerve fiber integrity is affected by stretching, this resulted in nerve fiber disruption and thus the nerve fibers began to lose their shape and began to fragment. This resulted in a decrease in the percent area of nerve fibers.

β APP is normal constituent of neurons that is transported by fast axonal transport and is known to be a useful marker for axonal damage because it accumulates at sites of focal axoplasmic transport impairment [16,26,37,38]. Although β APP is known to be a sensitive marker for identifying axonal injury, it is important to allow for the protein to accumulate post-injury. Previous studies showed that β APP accumulation appears as early as 3 hours post-injury and the amount of detected accumulation increased the longer the survival time post-injury [37,38]. Therefore, for this current study the BP terminal nerves were harvested 3 hours post-stretch to allow time for β APP to accumulate, if any, at the site of injury. In the current study, it was found that the percent area of positive β APP increased with strain in each of the BP terminal nerves. In addition, it was found that the amount of β APP accumulation was significantly different between the stretched nerves and sham of each BP terminal nerve. Singh et al. [26,27] using adult rat nerve roots demonstrated that the occurrence of β APP was strain and displacement rate dependent. Although the two previously reported studies cannot be directly compared to the current study, all these studies confirm that axoplasmic transport impairment increased and the occurrence of β APP and accumulation was strain dependent, respectively, such that β APP increased with increasing strain.

To determine if structural changes occurred throughout the peripheral nerve or localized to a specific location within the peripheral nerve, three longitudinal sections (two from the peripheries and one from the center) were examined for each of the three histological techniques. When examining vascular changes, nerve fiber changes, and extent of axoplasmic transport through β APP accumulation, there were no significant differences between the two peripheries and the center. Singh et al. [26,27] found similar results using adult rat nerve roots. Therefore, for these histological assessments it is assumed that the strain was uniformly distributed across the cross-section of the entire stretch nerve. However, when examining the extent of fascicle changes by measuring the nerve fiber area, significant differences were found between one periphery and the center of the ulnar BP terminal nerve.

Although the BP terminal nerves were grouped based on their actual strain as a result from the pre-determined strain testing (<10%, 10-20%, and >20%), the moderate stretch group which corresponds to 10-20% strains had a wide range. This can be attributed to segments along the BP terminal

nerves experiencing lower or higher strains since each BP terminal nerve bifurcate from various levels. However, greater structural changes were observed in 10-20% compared to the sham and <10% groups.

Conclusions

Using a clinically relevant neonatal piglet animal model, this study characterized an in-depth structural change in neonatal BP tissue at various strain ranges using various immuno-histological techniques. This study demonstrated vascular changes, nerve fiber changes, and extent of axoplasmic transport impairment increased with increasing strains. Additionally, this study found that as strains increased the area of nerve fiber decreased. This histological data at various strains can aid in the understanding of the injury mechanism of NBPP and thus help clinicians with diagnosis and prognosis of NBPP. The obtained data can also help establish a structural injury threshold for the neonatal BP. When combined with functional studies, a direct correlation can be established between electrophysiological and functional outcomes of BP injuries [39,40]. The reported study serves as a foundation to future studies that can further the understanding of neonatal BP injury mechanism and advance the science of neonatal care.

Acknowledgements

This project was supported by funding from the Eunice Kennedy Shriver National Institute of Child Health and Human Development of the National Institutes of Health under Award Number R15HD093024, R01HD104910A, and NSF CAREER grant Award #1752513.

Conflicts of Interest: No conflict of interest.

References

1. Abzug JMMD, Kozin SHMD. Current Concepts: Neonatal Brachial Plexus Palsy. *Orthopedics* 33 (2010): 430-435.
2. Abid A. Brachial plexus birth palsy: Management during the first year of life. *Orthopaedics & Traumatology: Surgery & Research* 102 (2016): S125-S132.
3. Zafeiriou DI, Psychogiou K. Obstetrical Brachial Plexus Palsy. *Pediatric Neurology* 38 (2008): 235-242.
4. Al-Qattan MM, El-Sayed AAF, Al-Zahrani AY, et al. Narakas Classification of Obstetric Brachial Plexus Palsy Revisited. *Journal of Hand Surgery-European Volume* 34E (2009): 788-791.
5. Johnson EO, Troupis T, Michalinos A, et al. Obstetrical brachial plexus palsy: lessons in functional neuroanatomy. *Injury* 44 (2013): 293-298.
6. Gonik B, Zhang N, Grimm MJ. Prediction of brachial plexus stretching during shoulder dystocia using a

- computer simulation model. *American Journal of Obstetrics and Gynecology* 189 (2003): 1168-1172.
7. Mehlman CT. Neonatal Brachial Plexus Palsy, in *The Pediatric Upper Extremity*. In: Abzug JM, Kozin SH, Zlotolow DA (Eds). Springer New York: New York, NY. (2015): pp: 589-605.
 8. Nikolaou S, Liangjun H, Tuttle LJ, et al. Contribution of denervated muscle to contractures after neonatal brachial plexus injury: not just muscle fibrosis. *Muscle & Nerve* 49 (2014): 398-404.
 9. Andersen J, Watt J, Olson J, et al. Perinatal brachial plexus palsy. *Paediatr Child Health* 11 (2006): 93-100.
 10. Heise CO, Martins R, Siqueira M. Neonatal brachial plexus palsy: a permanent challenge. *Arquivos De Neuro-Psiquiatria* 73 (2015): 803-808.
 11. Yang LJS. Neonatal brachial plexus palsy--management and prognostic factors. *Semin Perinatol* 38 (2014): 222-234.
 12. O'Berry P, Brown M, Phillips L, et al. Obstetrical brachial plexus palsy. *Curr Probl Pediatr Adolesc Health Care* 47 (2017): 151-155.
 13. Addas BM. Obstetric brachial plexus injury. *Neurosciences* 15 (2010): 136-137.
 14. Heise CO, Siqueira MG, Martins RS, et al. Motor nerve-conduction studies in obstetric brachial plexopathy for a selection of patients with a poor outcome. *JBJS* 91 (2009): 1729-1737.
 15. Simon NG, Franz CK, Gupta N, et al. Central Adaptation following Brachial Plexus Injury. *World Neurosurg* 85 (2016): 325-332.
 16. Hill CS, Coleman MP, Menon DK. Traumatic axonal injury: mechanisms and translational opportunities. *Trends in neurosciences* 39 (2016): 311-324.
 17. Bruggeman GF, Haitsma IK, Dirven CMF, et al. Traumatic axonal injury (TAI): definitions, pathophysiology and imaging—a narrative review. *Acta Neurochirurgica* 163 (2021): 31-44.
 18. Al-Sarraj S, Troakes C, Ruttly GN. Axonal injury is detected by β APP immunohistochemistry in rapid death from head injury following road traffic collision. *International Journal of Legal Medicine* 136 (2022): 1321-1339.
 19. Oehmichen M, Meissner C, Schmidt V, et al. Axonal injury—a diagnostic tool in forensic neuropathology?: A review. *Forensic science international* 95 (1998): 67-83.
 20. Warner WS, Yeoh S, Light A, et al. Rapid-stretch injury to peripheral nerves: histologic results. *Neurosurgery* 86 (2020): 437-445.
 21. Singh A, Shaji S, Delivoria-Papadopoulos M, et al. Biomechanical Responses of Neonatal Brachial Plexus to Mechanical Stretch. *Journal of brachial plexus and peripheral nerve injury* 13 (2018): e8-e14.
 22. Singh A, Orozco V, Balasubramanian S. In vivo biomechanical responses of neonatal brachial plexus when subjected to stretch. *PloS one* 18 (2023): e0290718.
 23. Singh A, Magee R, Balasubramanian S. Methods for In Vivo Biomechanical Testing on Brachial Plexus in Neonatal Piglets. *JoVE* 154 (2019): e59860.
 24. Hedrick TL. Software techniques for two- and three-dimensional kinematic measurements of biological and biomimetic systems. *Bioinspir Biomim* 3 (2008): 034001.
 25. Orozco V, Balasubramanian S, Singh A. Direct Linear Transformation for the Measurement of In-Situ Peripheral Nerve Strain During Stretching. *Journal of Visualized Experiments: Jove* 203 (2024).
 26. Singh A. Extent of impaired axoplasmic transport and neurofilament compaction in traumatically injured axon at various strains and strain rates. *Brain injury* 31 (2017): 1387-1395.
 27. Singh A, et al. Structural and functional changes in nerve roots due to tension at various strains and strain rates: an in-vivo study. *Journal of Neurotrauma* 26 (2009): 627-640.
 28. Gao Y, Weng C, Wang X. Changes in nerve microcirculation following peripheral nerve compression. *Neural Regeneration Research* 8 (2013): 1041.
 29. Mizisin AP, Weerasuriya A. Homeostatic regulation of the endoneurial microenvironment during development, aging and in response to trauma, disease and toxic insult. *Acta Neuropathologica* 121 (2011): 291-312.
 30. Topp KS, Boyd BS. Structure and biomechanics of peripheral nerves: nerve responses to physical stresses and implications for physical therapist practice. *Physical Therapy* 86 (2006): 92-109.
 31. Alvites R, et al. Peripheral nerve injury and axonotmesis: State of the art and recent advances. *Cogent Medicine* 5 (2018): 1466404.
 32. Flores AJ, Lavemia C, Owens PW. Anatomy and physiology of peripheral nerve injury and repair. *American Journal of Orthopedics-Belle Mead* 29 (2000): 167-178.
 33. Jou IM, Lai KA, Shen CL, et al. Changes in conduction, blood flow, histology, and neurological status following

- acute nerve-stretch injury induced by femoral lengthening. *Journal of Orthopaedic Research* 18 (2000): 149-155.
34. Kevenaar JT, Hoogenraad CC. The axonal cytoskeleton: from organization to function. *Frontiers in molecular neuroscience* 8 (2015): 44.
 35. Elmers J, Colzato LS, Akgün K, et al. Neurofilaments—Small proteins of physiological significance and predictive power for future neurodegeneration and cognitive decline across the life span. *Ageing Research Reviews* 90 (2023): 102037.
 36. Mahan MA, Warner WS, Yeoh S, et al. Rapid-stretch injury to peripheral nerves: implications from an animal model. *Journal of Neurosurgery* 133 (2019): 1537-1547.
 37. McKenzie KJ, McLellan DR, Gentleman SM, et al. Is β -APP a marker of axonal damage in short-surviving head injury? *Acta Neuropathologica* 92 (1996): 608-613.
 38. Gentleman S, Roberts GW, Gennarelli TA, et al. Axonal injury: a universal consequence of fatal closed head injury? *Acta Neuropathologica* 89 (1995): 537-543.
 39. Orozco V, Balasubramanian S, Singh A. A Systematic Review of the Electrodiagnostic Assessment of Neonatal Brachial Plexus. *Neurology and Neurobiology* 3 (2020).
 40. Tom B, Witko J, Lemay M, et al. Effects of bioengineered scaffold loaded with neurotrophins and locomotor training in restoring H-reflex responses after spinal cord injury. *Experimental Brain Research* 236 (2018): 3077-3084.